A Key to Improved Ion Core Confinement in the JET Tokamak:
Ion Stiffness Mitigation due to Combined Plasma Rotation and Low Magnetic Shear

P. Mantica,[1] C. Angioni,[2] C. Challis,[3] G. Colyer,[3] L. Frassinetti,[4] N. Hawkes,[3] T. Johnson,[4] M. Tsalas,[5] P. C. deVries,[6] J. Weiland,[7] B. Baiocchi,[1,8] M. N. A. Beurskens,[3] A. C. A. Figueiredo,[9] C. Giroud,[3] J. Hobirk,[2] E. Joffrin,[10] E. Lerche,[11] V. Naulin,[12] A. G. Peeters,[13] A. Salmi,[14] C. Sozzi,[1] D. Strintzi,[5] G. Staebler,[15] T. Tala,[16] D. Van Eester,[11] and T. Versloot[6]

[1]*Istituto di Fisica del Plasma "P. Caldirola," Associazione Euratom-ENEA-CNR, Milano, Italy*
[2]*Max-Planck-Institut für Plasmaphysik, EURATOM Association, Garching, Germany*
[3]*Euratom/CCFE Association, Culham Science Centre, Abingdon, OX14 3DB, United Kingdom*
[4]*Association EURATOM–VR, Fusion Plasma Physics, EES, KTH, Stockholm, Sweden*
[5]*Association EURATOM-Hellenic Republic, Athens, Greece*
[6]*FOM Institute Rijnhuizen, Association EURATOM-FOM, Nieuwegein, The Netherlands*
[7]*Chalmers University of Technology and Euratom-VR Association, Göteborg Sweden*
[8]*Università degli Studi di Milano, Department of Physics, Milano, Italy*
[9]*Associação Euratom-IST, Instituto de Plasmas e Fusão Nuclear, Instituto Superior Técnico, Lisboa, Portugal*
[10]*Association Euratom-CEA, CEA/IRFM, F-13108 Saint Paul Lez Durance, France*
[11]*LPP-ERM/KMS, Association Euratom-Belgian State, TEC, B-1000 Brussels, Belgium*
[12]*Association Euratom-Risø DTU, DK-4000 Roskilde, Denmark*
[13]*University of Bayreuth, 95440 Bayreuth, Germany*
[14]*Association EURATOM-Tekes, Aalto University, Department of Applied Physics, Finland*
[15]*General Atomics, P.O. Box 85608, San Diego, California 92186-5608, USA*
[16]*Association EURATOM-Tekes, VTT, P.O. Box 1000, FIN-02044 VTT, Finland*
(Received 13 May 2011; published 22 September 2011)

New transport experiments on JET indicate that ion stiffness mitigation in the core of a rotating plasma, as described by Mantica *et al.* [Phys. Rev. Lett. **102,** 175002 (2009)] results from the combined effect of high rotational shear and low magnetic shear. The observations have important implications for the understanding of improved ion core confinement in advanced tokamak scenarios. Simulations using quasilinear fluid and gyrofluid models show features of stiffness mitigation, while nonlinear gyrokinetic simulations do not. The JET experiments indicate that advanced tokamak scenarios in future devices will require sufficient rotational shear and the capability of q profile manipulation.

Ion temperature gradient (ITG) modes [1–4] are described by theory as featuring a threshold in the inverse ion temperature gradient length ($R/L_{T_i} = R|\nabla T_i|/T_i$, with R the tokamak major radius) above which the ion heat flux (q_i) increases strongly with R/L_{T_i}. This property leads to a level of stiffness of T_i profiles, characterizing how strongly they are tied to the threshold. The role of plasma rotation on threshold and stiffness is of high relevance for predicting the performance of future devices, because the core T_i and fusion power achievable for a given T_i pedestal depend crucially on threshold and stiffness [5] and future devices are expected to exhibit lower rotation than present devices from which scaling laws are derived.

The role of $E \times B$ flow shear stabilization [6] has been investigated in nonlinear gyrokinetic and fluid simulations [7–10] and found to result in a threshold upshift. From these studies the well-known "Waltz" quenching rule has been derived: $\gamma_{E \times B} = \gamma_{no E \times B} - \alpha_E \omega_{E \times B}$ where γ is the instability growth rate, $\omega_{E \times B}$ is the flow shearing rate and $\alpha_E \sim 1$ (see [9] for a recent revision). Experimentally, the only study of the impact of rotation on ion threshold and stiffness was performed on JET and reported in [11].

The unexpected result was found that in the plasma core the main effect of rotation is to lower the stiffness rather than increase the threshold, leading to significantly higher R/L_{T_i} in rotating plasmas, well above the levels expected by the threshold upshift foreseen by the Waltz rule.

This Letter presents new experimental results on the combined role of rotation and magnetic shear (s) in lowering ion stiffness, using transport tools such as q_i scans and T_i modulation in plasmas with different safety factor (q) and rotation profiles. The new empirical hypothesis is proposed that the concomitant presence of high rotational shear and low s is the condition for achieving ion stiffness mitigation in tokamaks. The relevance of the results for the improved ion core confinement observed in hybrid regimes [12] or ion internal transport barriers (ITBs) [13] is examined based on JET data. A comparison to state-of-art theory is finally presented, discussing quasilinear fluid and gyrofluid and nonlinear gyrokinetic models.

With reference to the main experiment discussed in [11] [q_i scan at $\rho_{tor} = 0.33$ by varying the localization of ion cyclotron resonance heating (ICRH) power in (^{3}He)-D minority], reported for the sake of comparison in
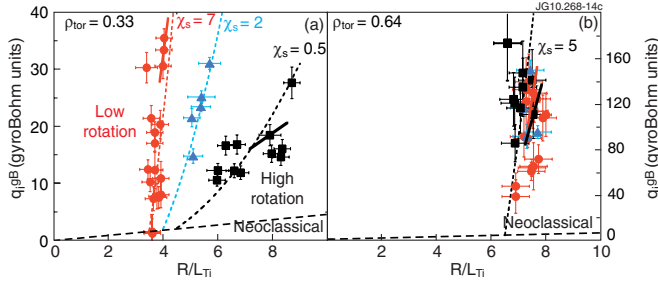
FIG. 1 (color online). q_i^{GB} $[= q_i/[(\rho_i/R)^2 v_{ith} n_i T_i]$
with $v_{ith} = (T_i/m_i)^{1/2}$, $\rho_i = (T_i m_i)^{1/2}/eB]$ vs R/L_{T_i} at
(a) $\rho_{tor} = 0.33$, (b) $\rho_{tor} = 0.64$ for similar plasmas with different
rotations. ●: $1 < \omega_{t0} < 2 \times 10^4$ rad/s; ▲: $3 < \omega_{t0} < 4 \times$
10^4 rad/s; ■: $5 < \omega_{t0} < 6 \times 10^4$ rad/s. The dashed black line
is indicative of neoclassical transport. The dotted lines represent
the critical gradient model (CGM) [11] with different values of χ_s.

Fig. 1(a), the analysis of the data at $\rho_{tor} = 0.64$ [Fig. 1(b)]
indicates that the stiffness reduction due to rotation (ob-
served at $\rho_{tor} = 0.33$) is not present. This is confirmed also
by T_i modulation data, which yield the slope of the curve as
indicated by the two segments. Besides higher values of
normalized q_i in the outer region, a major difference in
plasma parameters between the two regions is the magnetic
shear $s = \partial \ln q/\partial \ln \rho$, with $s > 1$ at $\rho_{tor} = 0.64$ while
$s \sim 0.4$–0.6 at $\rho_{tor} = 0.33$. The rotational shear instead
does not show a definite trend with radius. s is determined
by EFIT [14] with magnetic, pressure profile, and motional
Stark effect (MSE) or polarimeter constraints (statistical
error $\sim \pm 0.05$).

ICRH q_i scans at low and high rotation were carried
out in discharges with similar parameters as in Fig. 1's
data set (L mode, $B_T = 3.36$ T, $I_p = 1.8$ MA, $n_{e0} =$
3–4×10^{19} m^{-3}), but in which the q profile, and hence
s and s/q, were varied by lower hybrid preheat, plasma
current (I_p) ramp-up and ramp-down (1.8 to 3 MA in
3.5 s), I_p overshoot [12]. s was varied between 0.05 and
0.8 ($0.02 < s/q < 0.5$) at $\rho_{tor} = 0.33$ and between 0.75
and 1.45 ($0.25 < s/q < 0.7$) at $\rho_{tor} = 0.64$. The aim was
to investigate if a low s value is indeed a concomitant
requirement for stiffness reduction due to rotation. Ion
threshold and stiffness have been identified as in [11] by
placing on- and off-axis 3 MW of ICRH power in
(^{3}He)-D minority at concentrations $n_{^3He}/n_e \sim 6\%$–8%
and measuring R/L_{T_i} with active charge exchange spec-
troscopy. T_i modulation was performed on top. In the
high rotation discharges, up to 11 MW of coinjected
neutral-beam (NBI) power was applied. Figure 2(a)
shows the time evolution of the q profile in a low rotation
shot with I_p ramp-up and off-axis ICRH. s and s/q at
$\rho_{tor} = 0.33$ and 0.64 are shown vs time in Fig. 2(b). In
low NBI discharges, positioning ICRH off-axis implies
that the actual R/L_{T_i} at $\rho_{tor} = 0.33$ is a measure of
threshold, since $q_i \sim 0$. Therefore, the time evolution of
R/L_{T_i} directly yields the dependence of threshold
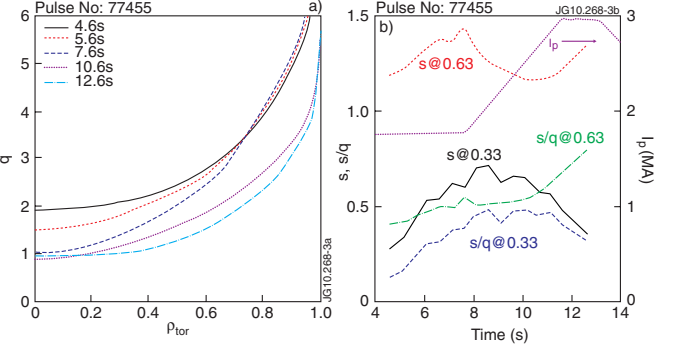on s/q, which is expected from linear theory to be

FIG. 2 (color online). (a) time evolution of MSE q profile for
pulse 77455; (b) I_p, s, s/q vs time at two radii.

stabilizing. Figure 3 shows R/L_{T_i} vs time at $\rho_{tor} = 0.33$
for the low and high rotation I_p ramp-up shots, and the
linear ITG threshold (similar for both shots) predicted by
an analytical formula proposed in [15]

$$R/L_{T_i}^{ITG} = \frac{4}{3}\left(1 + \frac{T_i}{T_e}\right)\left(1 + 2\frac{s}{q}\right) \text{ for } \frac{R}{L_n} < 2\left(1 + \frac{T_i}{T_e}\right). \quad (1)$$

The increase in measured threshold with time following
the increase of s/q is in good agreement with the ex-
pected dependence from Eq. (1). In spite of such threshold
increase, it is remarkable that the time behavior of R/L_{T_i}
in the high rotation shot is opposite, with R/L_{T_i} lying 3
times above threshold in the early phase and dropping to a
factor 1.3 of threshold at late times. At low rotation
instead also the on-axis ICRH case (not shown, but vir-
tually identical to the off-axis case) due to high stiffness
keeps close to threshold with R/L_{T_i} increasing with time.
This observation is a beautiful confirmation of the fact
that at high rotation the core T_i dynamics is completely
dominated by stiffness, and the stiffness reduction is more
pronounced when the q profile is flatter (i.e., at early
times). At outer radii, where stiffness is high irrespective
of rotation, R/L_{T_i} both at low and high rotation keeps
close to 7.5. The transport changes in Fig. 3 are accom-
panied by consistent changes in turbulence measured by
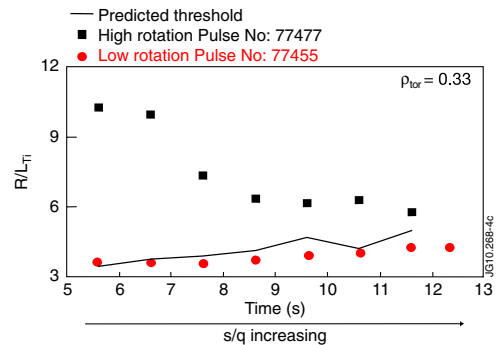correlation reflectometry [16], as discussed in [17].

FIG. 3 (color online). Experimental R/L_{T_i} at $\rho_{tor} = 0.33$ vs
time at low (red circles) and high (black squares) rotation for the
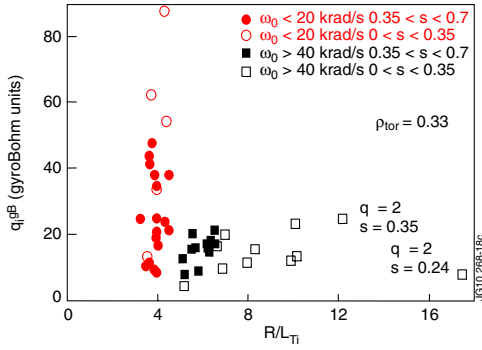I_p ramp-up case, and ITG threshold predicted with Eq. (1).

FIG. 4 (color online). q_i^{GB} vs R/L_{T_i} at $\rho_{tor} = 0.33$ for similar plasmas with different rotation and s values.

Similar observations are made with the other schemes for q profile variation. The data are summarized in Fig. 4. q_i values are estimated by the PION ICRH code [18], s is from MSE. Low rotation data show high stiffness irrespective of s, while at high rotation the stiffness reduction is larger at low s, allowing R/L_{T_i} up to 10 even at low q_i^{GB}.

Very high R/L_{T_i} (>10) is seen at high rotations when the $q = 2$ surface is at low s, while at higher s it does not lead to R/L_{T_i} increase. This is in line with observations of the beneficial role of low order rationals near $s = 0$ on turbulent transport [19–22], for which a theoretical basis was proposed in [23]. Such effect of rationals appears as a different phenomenon, which adds to the stiffness mitigation discussed in this Letter. In fact, the effect of rationals is reported both on ions and electrons [19–22] and also in the absence of rotation [19,22], while the stiffness mitigation is only observed on ions and strictly linked to rotation.

The evidence of ion stiffness reduction due to rotation and low s has profound implications on the interpretation of improved ion core confinement in hybrid plasmas or ion ITBs, proposing an alternative paradigm to the usual one based on $E \times B$ flow shear threshold up-shift. As a matter of fact, both regimes are experimentally observed in conditions of strong rotation and are lost in the absence of rotation [22,24]. Also, an important role of q profile manipulation is recognized experimentally (e.g., [12,13]). In [25] the role of both rotation and low s was already deduced from JET ITB experimental data. Figure 5 (inset) shows typical JET q profiles in 4 regimes: standard H mode with fully diffused current, hybrid, optimized shear (OS) and negative shear (NS) ITBs. Both hybrids and ITBs have core regions of very low s. Their position in the q_i^{GB} vs R/L_{T_i} plot at $\rho_{tor} = 0.33$ (Fig. 5) shows that the data populate uniformly the region of high R/L_{T_i} and low q_i^{GB}. Some considerations can be made to discriminate if this behavior is mainly due to stiffness or threshold.

In the core of hybrids the linear threshold was found between 3.5 and 5 using GS2 [26], well below the actual R/L_{T_i}. $\omega_{E \times B} \sim 3$–$4 \times 10^4$ s^{-1}, yielding threshold up-shifts ~ 1. The profiles then lie well above threshold even at small q_i^{GB}, indicating low stiffness. This was also confirmed by NBI T_i modulation (not shown). R/L_{T_i} vs s at
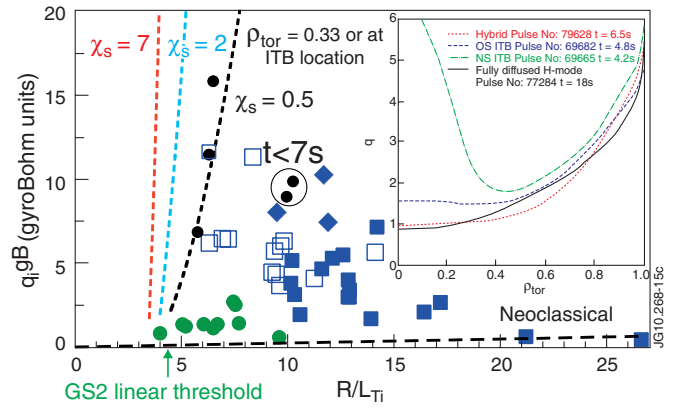

FIG. 5 (color online). q_i^{GB} vs R/L_{T_i} at $\rho_{tor} = 0.33$ for a set of hybrids (green or gray circles), ion ITBs at trigger time (blue open squares) and fully developed (blue full squares, diamonds with large ICRH fraction and reduced rotation). The data of Fig. 1(a) are indicated by CGM fits (dashed lines). Black circles are from pulse 77477 at different times (cf. Fig. 3). Neoclassical level and GS2 linear threshold for a hybrid are shown. The inset shows q profiles from MSE for the four scenarios.

low and high rotation is plotted in Fig. 6 from a JET H mode and hybrid database. The scatter is due to the range in parameters in the database, in first place q_i. Still, it is remarkable that the two clouds clearly separate at low s, with larger R/L_{T_i} at high rotation. This suggests that stiffness mitigation in the broad low s region is at the origin of the improved core ion confinement. The dependence on s is also one reason (together with different deposition profiles) why not much effect is seen in fully diffused H modes when ICRH power is substituted to NBI power [27].

For ITBs, the profiles at trigger yield $\omega_{E \times B} \sim$ 1–2×10^4 s^{-1}, not producing large threshold up-shift. The data lie in Fig. 5 in between the rotating shots of Fig. 1(a) and the neoclassical level. In fully developed ITBs, however, the ITB itself generates a large $\nabla \omega_t$ at the ITB radius, with $\omega_{E \times B} \sim 7$–$8 \times 10^4$ s^{-1}, inducing significant threshold up-shifts. It is then difficult to separate the role of threshold and stiffness. T_i modulation has been
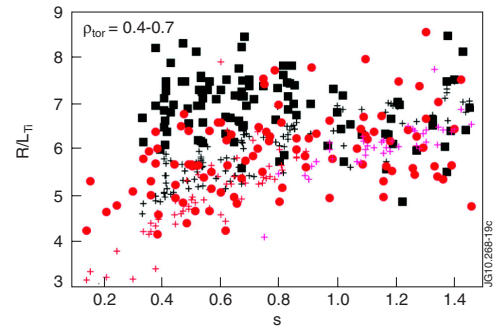

FIG. 6 (color online). R/L_{T_i} vs s at $\rho_{tor} = 0.4$–0.7 at low [red circles, $\nabla \omega_t < 50$ krad/(ms)] and high [black squares, $\nabla \omega_t >$ 130 krad/(ms)] rotation from a hybrid and H-mode JET database. s is from EFIT with polarimeter. Crosses are threshold values after Eq. (1).
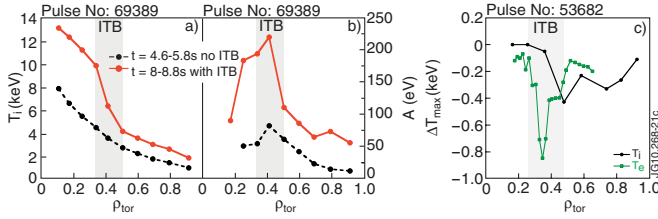
FIG. 7 (color online). (a) T_i, (b) amplitudes for an ITB
shot before trigger (black dashed line) and at full strength (red
full line). (c) Ion and electron cold pulse maximum amplitude.

performed using ^{3}He ICRH modulation. T_i and amplitude
profiles with and without ITB are compared in Figs. 7(a)
and 7(b). The ITB acts as a layer of low incremental
diffusivity, with sharp variation of amplitudes, indicating
a low slope of the q_i vs R/L_{T_i} plot. These observations,
reported also for electrons in [28], are not consistent with
T_i profiles tight to a high threshold by high stiffness, but
rather with either transport above critical with low stiff-
ness, or with subcritical transport. The second hypothesis
must be discarded because in most cases ITBs and hybrids
are found well above neoclassical (Fig. 5). We conclude
that also in ion ITBs the pattern of decreasing stiffness
plays a major role, with the threshold up-shift intervening
in a nonlinear feedback while the ITB develops. Such a
picture for ions is different from that for electrons pro-
posed in [28], with electron ITBs as subcritical regions in
the presence of stiff electron transport. The difference is
confirmed by the behavior of electron and ion cold pulses
when they meet the ITB propagating from edge [Fig. 7(c)].
The electron cold pulse grows significantly inside the ITB
[28], due to redestabilization of stiff turbulent transport
[29]. For ions, with low stiffness in the ITB, the cold pulse
growth cannot take place but strong damping is seen.

While in ITB plasmas the H factor ~ 1.5 is all due to large
core gradients, in hybrids enhanced pedestal and neoclassical
tearing mode (NTM) stabilization also contribute to the H
factor. It was shown statistically [30] that the contribution of
pedestal to total energy is 20%–40% both in H modes and
hybrids and that the H factor up to 1.5 in hybrids is due in
equal parts to core and pedestal improvement, with the core
part mainly in the ion channel. These findings are consistent
with our estimate that an increase in R/L_{T_i} from 6 to 10 due
to stiffness mitigation in a region up to $\rho_{\rm tor} = 0.6$ at fixed
pedestal leads to $\Delta H \sim 0.2$. With regard to NTMs, experi-
ments show [31] that strong NTM onset leads to an abrupt
drop of the H factor to ~ 1, with a deterioration of T_i profile
mainly caused by the braking of plasma rotation. This does
not contradict the fact that, when NTMs are weak or absent,
the core transport dynamics discussed above are at play.

Finally, we address the state of the art of theory predictions
on the effect of rotation on ion transport. In widely used
quasilinear transport models, such as WEILAND [32] or GLF23
[33], which apply the Waltz rule on a given and restricted
choice of spectral wave numbers, rotation introduces only a
small threshold up-shift and not a change in slope. The results
by the WEILAND model for a shot with $s = 0.57$ are shown in
Fig. 8(a) without and with rotation [$\gamma_E = \omega_{E \times B}/c_s/a \sim 0.1$,
with $c_s = (T_e/m_i)^{1/2}$]. On the other hand, the more recent
gyrofluid TGLF model [34], which makes use of full spectra,
indicates a change in slope [Fig. 8(b)], in particular, in the
region of the knee, at the transition between fully developed
turbulence and zonal flows. The simulations scan R/L_{T_i} and
R/L_{T_e} in a prescribed ratio (from experiment) without and
with rotation. This effect may be due to differential suppres-
sion of turbulence at various wavelengths, with more suppres-
sion of the low stiffer ones. The change in stiffness with
rotation is larger at low s [Fig. 8(d)] as in experiments. The
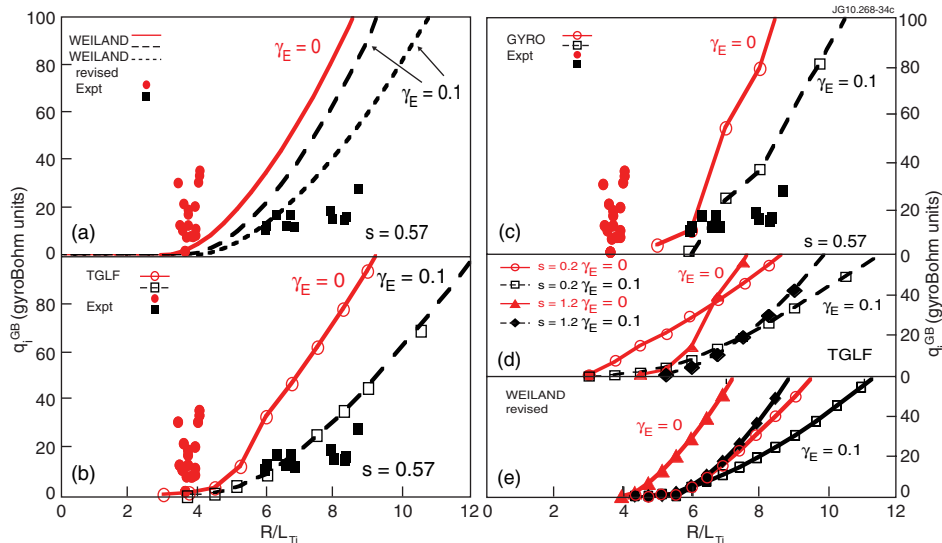WEILAND model has been modified to include the dependence

FIG. 8 (color online). $q_i^{\rm GB}$ vs R/L_{T_i} at $\rho_{\rm tor} = 0.33$ without and with rotation from (a) WEILAND, (b) TGLF, and (c) GYRO simulations
with $s = 0.57$ compared with the data of Fig. 1(a). (d) TGLF and (e) revised WEILAND [legend as in (d)] simulations with
$s = 0.2$ and 1.2.

of the fastest growing mode number on rotation [35], obtaining results very similar to TGLF [Figs. 8(a) and 8(e)].

To verify these results, nonlinear flux-tube electrostatic gyrokinetic simulations using GYRO [36] have been made [Fig. 8(c)], with background rotation and electron-ion collisions, for the same parameters as with TGLF. The box size is $62 \times 222 \, \rho_s$ ($\rho_s = (T_e m_i)^{1/2}/eB$) with 64 toroidal modes from $k_y \rho_s = 0.028$ to $k_y \rho_s = 1.78$ and with a minimum $k_x \rho_s = 0.1$ and max $k_x \rho_s = 6.47$ corresponding to a radial resolution $\delta x / \rho_s = 0.24$. The radial box size is $\Delta r / a = 0.125$. At low R/L_{T_i}, very large $n = 0$ (zonal) electrostatic potential fluctuations are found, which strongly reduce the transport and obligate us to perform simulations exceeding $1000 a / c_s$. The same results are obtained with double radial box size keeping the same radial resolution. We note that runs with a reduced number of toroidal modes do not deliver the same strength of zonal flows. With 64 modes, due to the large zonal flows, turbulent transport is rapidly quenched to zero near threshold and there is no hint of stiffness mitigation at high rotation, but basically only a threshold up-shift. Similar results were obtained with GKW [37] as reported in [17] and recently with GS2 on a different case [[38], Fig. 3(a)]. Global simulations did not yield significant changes at this inner radius. Since the mechanisms mentioned above as a possible origin of the stiffness reduction in quasilinear models are also included, and with most resolved treatment, in nonlinear gyrokinetic models, we have to admit that presently the impact of rotation on ion stiffness remains an open issue on the theory side. It deserves further work because, although numerically challenging, the marginality region is the operating domain of fusion devices. We also note that none of the models in Fig. 8 in fact reproduce correctly the low R/L_{T_i} of the low rotation data, either due to not high enough stiffness or to the presence of a nonlinear (Dimits) threshold up-shift. This is also an open issue.

In summary, JET experiments show that ion stiffness is reduced by low s and high rotation. This indicates that advanced tokamak scenarios in future devices will require sufficient rotational shear and the capability of q profile manipulation.

[1] N. Mattor *et al.*, Phys. Fluids **31**, 1180 (1988).
[2] F. Romanelli *et al.*, Phys. Fluids B **1**, 1018 (1989).
[3] J. W. Connor and H. R. Wilson, Plasma Phys. Controlled Fusion **36**, 719 (1994).
[4] M. Kotschenreuther *et al.*, Phys. Plasmas **2**, 2381 (1995).
[5] B. Baiocchi *et al.*, Plasma Phys. Controlled Fusion (to be published).
[6] H. Biglari *et al.*, Phys. Fluids B **2**, 1 (1990).
[7] J. E. Kinsey *et al.*, Phys. Plasmas **12**, 062302 (2005).
[8] R. E. Waltz *et al.*, Phys. Plasmas **1**, 2229 (1994).
[9] J. E. Kinsey *et al.*, Phys. Plasmas **14**, 102306 (2007).
[10] X. Garbet *et al.*, Phys. Plasmas **9**, 3893 (2002).
[11] P. Mantica *et al.*, Phys. Rev. Lett. **102**, 175002 (2009).
[12] J. Hobirk *et al.*, Plasma Phys. Controlled Fusion (to be published).
[13] R. C. Wolf, Plasma Phys. Controlled Fusion **45**, R1 (2003).
[14] L. L. Lao *et al.*, Fusion Sci. Technol. **48**, 968 (2005) [http://www.new.ans.org/pubs/journals/fst/a_1052].
[15] S. C. Guo and F. Romanelli, Phys. Fluids B **5**, 520 (1993).
[16] A. C. A. Figueiredo *et al.*, in *Proceedings of the 36th EPS Conference, Sofia, 2009*, Europhysics Conference Abstracts, Vol. 33E, P-2.167, http://epsppd.epfl.ch/Sofia/pdf/P2_167.pdf.
[17] P. Mantica *et al.*, in *Proceedings of the 23rd IAEA Fusion Energy Conference, Daejeon, 2010* (IAEA, Vienna, 2010), EXC/9-2 [http://www-pub.iaea.org/mtcd/meetings/PDFplus/2010/cn180/cn180_papers/exc_9-2.pdf].
[18] L.-G. Eriksson *et al.*, Nucl. Fusion **33**, 1037 (1993).
[19] N. J. Lopes Cardozo *et al.*, Plasma Phys. Controlled Fusion **39**, B303 (1997).
[20] M. E. Austin *et al.*, Phys. Plasmas **13**, 082502 (2006).
[21] E. Joffrin *et al.*, Nucl. Fusion **42**, 235 (2002).
[22] P. C. de Vries *et al.*, Nucl. Fusion **49**, 075007 (2009).
[23] R. E. Waltz *et al.*, Phys. Plasmas **13**, 052301 (2006).
[24] P. A. Politzer *et al.*, Nucl. Fusion **48**, 075001 (2008).
[25] T. Tala *et al.*, Plasma Phys. Controlled Fusion **43**, 507 (2001).
[26] M. Kotschenreuther *et al.*, Comput. Phys. Commun. **88**, 128 (1995).
[27] T. W. Versloot *et al.*, Nucl. Fusion (to be published).
[28] P. Mantica *et al.*, Phys. Rev. Lett. **96**, 095002 (2006).
[29] A. Casati *et al.*, Phys. Plasmas **14**, 092303 (2007).
[30] L. Frassinetti *et al.*, in *Proceedings of the 37th EPS Conference, Dublin, 2010*, Europhysics Conference Abstracts, Vol. 34A, P-1.1031, http://ocs.ciemat.es/EPS2010PAP/pdf/P1.1031.pdf.
[31] C. D. Challis *et al.*, in *Proceedings of the 36th EPS Conference, Sofia, 2009*, Europhysics Conference Abstracts, Vol. 33E, P-5.172, http://epsppd.epfl.ch/Sofia/pdf/P5_172.pdf.
[32] J. Weiland, *Collective Modes in Inhomogeneous Plasmas* (IOP, Bristol, 2000).
[33] R. E. Waltz *et al.*, Phys. Plasmas **4**, 2482 (1997).
[34] G. M. Staebler *et al.*, Phys. Plasmas **12**, 102508 (2005).
[35] J. Weiland *et al.*, in Proceedings of 38th EPS Conference, Strasbourg, 2011, Europhysics Conference Abstracts, P-5.130, http://ocs.ciemat.es/EPS2011PAP/pdf/P5.130.pdf (to be published).
[36] J. Candy and R. E. Waltz, J. Comput. Phys. **186**, 545 (2003).
[37] A. G. Peeters *et al.*, Comput. Phys. Commun. **180**, 2650 (2009).
[38] E. G. Highcock *et al.*, Phys. Rev. Lett. **105**, 215003 (2010).
[39] F. Romanelli *et al.*, in *Fusion Energy 2010: Proceedings of the 23rd International Conference, Daejeon, 2010* [International Atomic Energy Agency (IAEA), Vienna, 2010] [http://www-pub.iaea.org/mtcd/meetings/PDFplus/2010/cn180/cn180_papers/ov_1-3.pdf]. (All the members of the JET-EFDA Collaboration appear in the appendix of this paper.)